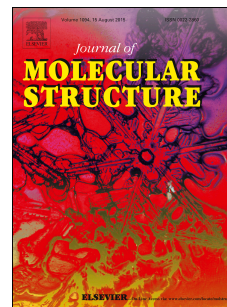


Accepted Manuscript

A structural study of fentanyl by DFT calculations, NMR and IR spectroscopy

Zahra Asadi, Mehdi D. Esrafil, Esmail Vessally, Manzarbanou Asnaashariisfahani, Saeideh Yahyaei, Ali Khani



PII: S0022-2860(16)30954-1

DOI: [10.1016/j.molstruc.2016.09.027](https://doi.org/10.1016/j.molstruc.2016.09.027)

Reference: MOLSTR 22939

To appear in: *Journal of Molecular Structure*

Received Date: 4 May 2016

Revised Date: 9 September 2016

Accepted Date: 9 September 2016

Please cite this article as: Z. Asadi, M.D. Esrafil, E. Vessally, M. Asnaashariisfahani, S. Yahyaei, A. Khani, A structural study of fentanyl by DFT calculations, NMR and IR spectroscopy, *Journal of Molecular Structure* (2016), doi: 10.1016/j.molstruc.2016.09.027.

This is a PDF file of an unedited manuscript that has been accepted for publication. As a service to our customers we are providing this early version of the manuscript. The manuscript will undergo copyediting, typesetting, and review of the resulting proof before it is published in its final form. Please note that during the production process errors may be discovered which could affect the content, and all legal disclaimers that apply to the journal pertain.

A structural study of fentanyl by DFT calculations, NMR and IR spectroscopy

Zahra Asadi^{*a}, Mehdi D. Ebrahimi^{*b}, Esmail Vessally^c, Manzarbanou Asnaashariifahani^d, Saeideh Yahyaei^e, Ali Khani^e

^a Young Researchers and Elite Club, Miyaneh Branch, Islamic Azad University, Miyaneh, Iran

^b Laboratory of Theoretical Chemistry, Department of Chemistry, University of Maragheh, Maragheh, Iran

^c Department of Chemistry, Payame Noor University, Tehran, Iran

^d Department of Chemistry, Islamic Azad University, North Tehran Branch, Tehran, Iran

^e Department of Chemistry, Miyaneh branch, Islamic Azad University, Miyaneh, Iran

* Corresponding Author. z.asadi161@gmail.com (Z. Asadi) and esrafil@maragheh.ac.ir (M.D. Ebrahimi).

Abstract

N-(1-(2-phenethyl)-4-piperidinyl)-N-phenyl-propanamide (fentanyl) is synthesized and characterized by FT-IR, ¹H NMR, ¹³C NMR, mass spectroscopy and elemental analyses. The geometry optimization is performed using the B3LYP and M06 density functionals with 6-311+G(d) and 6-311++G(d,p) basis sets. The complete assignments are performed on the basis of the potential energy distribution (PED) of the all vibrational modes. Almost a nice correlation is found between the calculated ¹³C chemical shifts and experimental data. The frontier molecular orbitals and molecular electrostatic potential of fentanyl are also obtained.

Keywords: opiate agonists; DFT; chemical shifts; M06; B3LYP; MEP.

1. Introduction

Opiate agonists such as 4-anilidopiperidine derivatives play a significant role in different alleviation of pain such as post operational, cancer, etc., and are often used in surgical analgesia and sedation [1,2]. N-(1-(2-phenethyl)-4-piperidinyl)-N-phenyl-propanamide (fentanyl) is an extremely powerful opioid analgesic from this family, which is about 50-100 times more potent than morphine in humans and is described as having a fast onset and a short duration of action [3].

Due to the importance of fentanyl in the biomedical fields, several synthetic routes have been suggested for its preparation [4-10]. Most of these methods, however, require multiple steps and lengthy refluxing reaction conditions. The isolation and purification of the intermediate compounds are both tedious, and time and energy consuming process. In addition, it may also reduce overall yield. The aim of this work is to develop an efficient method for preparation of fentanyl via an one-pot reaction that involves tandem reductive alkylation and amination reactions in the presence of sodium triacetoxyborohydride (STAB) followed by N-acylation reaction (Scheme 1). Sodium triacetoxyborohydride is mainly used as a mild and selective reducing agent. Also this reagent is especially suitable for reductive amination of aldehydes and ketones [11]. The structural characterization of fentanyl is also investigated using different experimental and theoretical methods. The theoretical studies are performed by means of two restricted density functional theory (DFT) methods, i.e. B3LYP and M06 functionals.

2. Experimental

2.1 General method

The reactions were monitored by TLC and NMR techniques, which indicated that there were no side products. The TLC plates were prepared from Merck silica gel powder. Melting points were obtained in open capillary tubes and were measured on an electro-thermal 9200 apparatus. IR spectra were measured on a Perkin-Elmer RXI, FT-IR spectrometer. ^1H and ^{13}C NMR spectra (CDCl_3) were recorded on a Bruker 300 DRX Avance instrument at 500.0 and 100.0MHz, respectively. Mass spectra were recorded on a Shimadzu QP 1100 BX mass spectrometer. The elemental analysis was performed by using a Perkin-Elmer 2400(II) CHN/O analyzer. The synthetic route is shown in Scheme 1.

< Scheme 1 >

2.2. Synthesis

To a stirred suspension of 4-piperidone monohydrochloride (15.36 g, 0.1 mol) in dichloroethane (450 ml), triethylamine (27.87 ml, 0.2 mol) and phenylacetaldehyde (11.17 ml, 0.1 mol) were added and stirred for half an hour at room temperature under N₂. Thereafter, sodium triacetoxyborohydride (30 g, 0.14 mol) was added to the reaction mixture with continuous stirring. The reaction mixture was further stirred for 24 h. Aniline (9.12 ml, 0.1 mol), acetic acid (11.53 ml, 0.2 mol) and sodium triacetoxyborohydride (30 g, 0.14 mol) were then added and again the reaction mixture was stirred for 24 h. Propionyl chloride (26.16 ml, 0.3 mol) was then added dropwise and the mixture was stirred for 2 h. The reaction mixture was then diluted with dichloromethane and washed with 4% aqueous sodium hydroxide solution followed by water. The organic phase was then shaken with 2N HCl. The organic layer was separated and the aqueous layer was extracted with DCM. Combined organic phase was dried over sodium sulfate and concentrated to give crude HCl salt of fentanyl. Crude product was recrystallized with acetone to give white powder of fentanyl hydrochloride. The salt was treated with 20% NaOH to give fentanyl which was recrystallized from petroleum ether (bp 60-80 °C). Characterization data are given below.

White powder; mp: 69-70°C. Yield: 81%. IR (KBr) (mmax, cm⁻¹): 3057, 1656, 744. ¹H NMR (500 MHz, CDCl₃) δ_H: 7.42–7.10 (m, 10H, arom); 4.71 (m, 1H); 3.05–3.03 (m, 2H); 2.78–2.75(m, 2H); 2.59–2.56 (m, 2H); 2.23–2.18 (t, 2H, J=11.3Hz); 1.98–1.93 (q, 2H, J=7.44Hz); 1.85–1.83 (m, 2H); 1.49–1.47 (m, 2H); 1.06–1.03 (t, 3H, J=7.44Hz). ¹³C NMR (CDCl₃) δ_C: 173.50; 140.24; 138.85; 130.41; 129.24; 128.59; 128.34; 128.21; 125.98; 60.46; 53.08; 52.14; 33.82; 30.56; 28.49; 22.57; 9.58. MS: m/z (%) (EI) 338 (M⁺, 1), 245 (7.5), 188 (2.5), 189 (5), 146 (12.5), 91(80), 77(42), 57(100). Anal. Calcd for C₂₂H₂₈N₂O: C, 78.53; H, 8.39; N, 8.33. Found: C, 78.42; H, 8.05; N, 8.62.

3. Computational details

In the present work, quantum chemical calculations were carried out at different DFT levels using the Gaussian 03 suites of programs [12]. The structure of fentanyl was optimized using the M06 and B3LYP density functionals employing 6-311+G(d) and 6-311++G(d,p) standard basis sets. No symmetry constraints were used during the optimization. Harmonic frequencies were calculated for this optimization to confirm the existence of a minimum (no imaginary frequencies) structure. The M06 is a hybrid meta-GGA functional, where the Hartree–Fock exchange energy is equal to 27% [13]. This density functional has been parameterized including main group atoms and transition metals, and it implicitly accounts for “medium-range” electron correlation. The isotopic chemical shielding (σ_{iso}) values were

calculated based on the gauge-independent atomic orbital (GIAO) approach [14]. The ^1H and ^{13}C chemical shifts (δ) were then calculated by subtracting the calculated isotopic value of the shielding tensor $\sigma_{iso,cal}$ from that of TMS: $\delta = \sigma_{iso,TMS} - \sigma_{iso,cal}$. Also, ^1H and ^{13}C chemical shifts of structure were simulated using the GaussView software [15]. The density of states plots were obtained using the GaussSum program [16]. The molecular electrostatic potential (MEP) analysis was performed on the 0.001 electrons/Bohr³ contour of the electronic density using the wave function analysis-surface analysis suite (WFA-SAS) [17].

4. Results and Discussion

4.1. Geometry and atomic charges

The optimized structure of fentanyl is shown in Figure 1. Tables 1-3 list calculated bond lengths, bond angles and dihedral angles at different levels of theory. The corresponding experimental data are also given for comparison. In each case, the true minimum structure is confirmed following an inspection of the frequencies and the IR spectra obtained after the frequency calculation. The inspection of the data presented in these Tables 1 reveals that the estimated bond lengths at different DFT levels are almost independent of the method and basis set used. Unless otherwise noted, the following results are referred for the B3LYP/6-311++G(d,p) and M06/6-311++G(d,p) levels of theory.

< Figure 1 >

The experimental carbon-carbon bond lengths of the phenyl group and piperidine ring of fentanyl are in the range of 1.38–1.40 and 1.52–1.54 Å, respectively [18, 19]. The B3LYP/6-311++G(d,p) and M06/6-311++G(d,p) methods predict these bond lengths in the range of 1.39–1.40, 1.53–1.54 Å and 1.38–1.39, 1.52–1.53 Å, respectively. In addition, the computed bond length of C18–C19 (1.54 Å) at the B3LYP/6-311++G(d,p) level is in good agreement with the experimental value reported in Table 1. The B3LYP/6-311++G(d,p) calculations predict the C8–O9 (1.22 Å), C18–N15 (1.45 Å), C12–N7 (1.48 Å), C8–N7 (1.37 Å), whereas at the M06/6-311++G(d,p) level, these bond lengths are 1.21, 1.44, 1.47, 1.37 Å, respectively. The correlations between the experimental and calculated bond lengths are shown in Figure 2. As is evident, almost a good linear correlation is obtained between the B3LYP/6-311++G(d,p) results and experimental data. This may indicate that the inclusion of “medium-range” electron correlation in the M06 density functional does not have any significant influence on the geometry of fentanyl. The estimated bond angles of C20-C19-

C18, C19-C18-N15, N15-C16-C17, C16-C17-C12, C17-C12-C13 are 111.9° (110.8°) 113.2° (113.4°), 110.1° (111.9°), 110.6° (109.7°), 110.3° (110.5°) at the B3LYP (M06) level, respectively, which are consistent with the experimental data [18, 19]. (Table 2). The calculated dihedral angles at B3LYP (M06) level for C16-C17-C12-C13, C18-N15-C14-C13 and C12-N7-C1-C2 are -62.1° (-62.8°), 162.0° (163.2°) and -80.7° (-80.6°), respectively, which are in good agreement with the corresponding experimental values of -54.4° , 167.9° and -96.3° [19, 20].

<Table 1>

<Table 2>

<Table 3>

<Figure 2>

The calculated Mulliken atomic charges of fentanyl are given in Figure 3 and Table 4. Except for N7, C13, N15, C20, C2, C6 and C21, all atoms are negatively charged. The largest value of positive charge is located on the C20 atom, ca. 1.047 e (0.740 e) at the B3LYP (M06) level. On the other hand, the C12 atom has the most negative charge -0.853 e (-1.570 e) at the B3LYP (M06) level. Besides, the results of Table 4 clearly indicate that the calculated atomic charges with the M06 level are almost smaller in comparison with those obtained by the B3LYP, regardless of the basis set used. For a given density functional, the addition of polarization and diffuse functions to the 6-311+G(d) basis set has a significant influence on the calculated atomic charges. As also evident from Figure 3, the dipole moment of fentanyl is oriented perpendicular relative to the piperidine ring. The calculated dipole moment value (3.2 Debye at both B3LYP and M06 levels) clearly indicate the partial ionic character of the C=O as well as the C-N bonds and verifies the relatively large charge density distribution within this molecule.

< Figure 3>

<Table 4>

4.2. Vibrational assignments

The experimental (FT-IR) and simulated vibrational spectra of fentanyl are shown in Figure 4. According to the theoretical calculations, fentanyl has the C1 point group symmetry. This compound consists of 53 atoms. The number of vibration normal modes

of fentanyl is 153 normal vibrational modes, 105 modes of vibrations are in-plane and 47 modes are out-of-plane. The bands that are in the plane of the molecule are represented as A', while out of the plane bands are assigned as A". Thus, the 153 normal modes of vibrations of fentanyl are distributed as $\Gamma_{\text{vib}} = 105A' + 47A''$. The theoretical frequencies and infrared intensities of fentanyl calculated at the B3LYP/6-311++G(d,p) and M06/6-311++G(d,p) levels are presented in Table S1 of Supporting Information. As expected, in all cases, the calculated harmonic frequencies are overestimated relative to experiment. This is mainly due to the harmonic approximation and may be due to the incomplete treatment of electron correlation in these calculations. Thus, to aid comparison between the theoretical and experimental frequencies, a scaling factor was used for the calculated frequencies [21]. As follows from this comparison, both the B3LYP and M06 methods provide good overall agreement with experiment. As Figure 5 indicates, almost a linear correlation is found between the experimental and calculated stretching frequencies of fentanyl at both M06 and B3LYP levels. Nevertheless, the careful examination of the results in Table S1 indicates that the calculated frequencies with the B3LYP method are closer to experimental values than those obtained by the M06 method. Besides, most of the frequencies calculated by the M06 method are larger than those of B3LYP ones, an observation reported previously for other related systems [22-25].

< Figure 4 >

< Figure 5 >

4.2.1. C–H vibrations

The C–H stretching vibration in alkanes and aromatic structures are in the regions of 2850–3000 cm^{-1} and 3000–3100 cm^{-1} , respectively [26, 27]. The FT-IR bands for the C–H stretching vibrations are observed at 3057 cm^{-1} . The calculated C–H stretching vibration appears at 3054.63 cm^{-1} at the B3LYP/6-311++G(d,p) level which is in good agreement with the experimental data (3057 cm^{-1}). The calculated C–H stretching vibrations appear at 2966 cm^{-1} by the M06/6-311++G(d,p) method.

As evidenced by the PED, this mode (mode no. 9) involves the contribution of 98%.

4.2.2. C=O vibrations

The C=O bond in esters is assigned in the region of 1730-1750 cm^{-1} [27]. In this structure, the C=O stretching vibration is seen at 1656 cm^{-1} . The calculated C=O stretching vibration appears at 1656.65 cm^{-1} using the B3LYP/6-311++G (d,p) level which is closer to the corresponding experimental data (1656 cm^{-1}). However, the M06 method gives a relatively larger deviation (17 cm^{-1}) from the experimental value. Helios et al. [28] have reported a similar effect for the B3LYP-and M06-calculated vibration stretching frequency of the carbonyl group in a polymeric Cu(II)-orotate complex. This is most likely due to the fact that the M06 functional usually overestimates the strength of the C=O bond, which leads to a shorter C=O bond length relative to those of B3LYP method and the predicted C=O stretching frequency is thus larger than experimental. We note, however, that Scuseria [29] and co-workers have attributed this behavior to the relatively larger percentage of Hartree-Fock exchange energy in the M06 functional (20%) than in the B3LYP (20%).

This mode (mode no. 29) involves the contribution of 83%, as indicated by the PED.

4.2.3. C-N vibrations

The C-N stretching absorption of amines occurs in the region of 1000-1250 cm^{-1} [27]. In this structure, the C-N bond is observed at 1244 cm^{-1} .

The calculated C-N stretching vibration appears at 1228.44 cm^{-1} using the B3LYP/6-311++G(d,p) level which was in good agreement with the experimental value. The calculated C-N stretching vibration appears at 1199.85 cm^{-1} at the M06/6-311++G(d,p) level.

As indicated by the PED, this mode (mode no. 66) involves the contribution of 12%.

4.3. Chemical shift analysis

Figure 6 shows the experimental ^1H NMR spectra of fentanyl. Theoretical simulation of ^1H chemical shifts were performed by the GaussView software which is shown in Figure S1. Table 5 lists the experimental and theoretical chemical shifts of ^1H nuclei in fentanyl. It is found that the ^1H chemical shifts (with respect to TMS) occur at 0.58–7.71 and 1.33–8.60 ppm at the B3LYP and M06 levels, respectively, whereas the experimental shifts are in the range of 1.03–7.42 ppm. The methyl protons (H33-H35) experimentally resonate at 1.03–1.06 ppm as a multiplet which these chemical shifts are theoretically predicted in the range of 0.58–1.24 ppm and 1.33–2.00 at the B3LYP and M06 levels, respectively. The signal in the range of 1.93–3.05 ppm is assigned to methylene protons (H37-H48 and H31, H32). The H36 proton of the title compound experimentally shows a multiplet at 4.71 ppm. This chemical shift theoretically occurs at 3.42 and 4.02 ppm at the B3LYP and M06 levels of theory,

respectively. The multiplet at 7.10–7.42 ppm corresponds to the aromatic protons (H26-30, H49-53) that are calculated at 7.30–7.71 and 7.95–8.60 ppm by B3LYP and M06, respectively. As Figure 7 indicates, H36 and H44 atoms indicate the largest $\delta_{\text{exp}}-\delta_{\text{cal}}$ value at both B3LYP and M06 levels. More especially, the average absolute standard deviation of the calculated ^1H NMR chemical shifts is calculated to be 0.44 and 0.79 at the B3LYP and M06 levels.

<Figure 6>

<Table 5>

< Figure 7>

The ^{13}C chemical shifts (with respect to TMS) are assigned in the range of 10.93–178.92 and 10.62–183.00 ppm by B3LYP and M06 methods, respectively, while the corresponding experimental data are observed in the range of 9.58–173.5 ppm (Figure 6 and Table 6). The largest deviation between the calculated and experimental ^{13}C NMR chemical shifts ($\delta_{\text{exp}}-\delta_{\text{cal}}$) is seen for C19 with -8.51 and -8.23 ppm at the B3LYP and M06 levels, respectively. The chemical shifts of C11, C17, C13 and C10 atoms are experimentally located at 9.58, 22.57, 28.49 and 30.56 ppm, respectively. The theoretical chemical shifts of these atoms are assigned at 10.93 (error approx. -1.35 ppm), 28.04 (error approx. -5.47 ppm), 31.11 (error approx. -2.62 ppm) and 34.25 (error approx. -3.69 ppm) at the B3LYP, and 10.62 (error approx. -1.04 ppm), 27.95 (error approx. -5.38 ppm), 28.08 ppm (error approx. 0.41 ppm) and 33.07 ppm (error approx. -2.51 ppm) at the M06 level. As Figure 7 indicates, the largest deviation of the calculated ^{13}C chemical shifts from the experimental values is seen for the C20 and C8 atoms. Besides, the average absolute standard deviation of ^{13}C chemical shifts is 5.2 and 5.5 at the B3LYP and M06 levels, respectively. This clearly indicates the larger deviation of ^{13}C chemical shifts from the experimental data than those of ^1H chemical shifts.

<Table 6>

The relationship between the experimental and computed chemical shifts of ^1H and ^{13}C NMR is shown in Figure 8. As evident, the correlation between the experimental and calculated chemical shifts is better for ^{13}C atoms than for ^1H atoms. This discrepancy can be expected since the ^1H chemical shifts were more sensitive to solvent effects [30]. As seen in Figure 8, the squared correlation coefficients (R^2) values obtained at the B3LYP level are slightly larger than those of at the M06 level. This indicates that for the system under study,

the B3LYP provides more reliable ^{13}C chemical shifts than the M06, may be due to the proper description of the structure of this molecule by the former density functional.

<Figure 8>

4.4. Frontier molecular orbital analysis

Density of states (DOS) diagram was obtained from the molecular orbital data and plotted by the GaussSum program [16]. The DOS diagram of fentanyl is shown in Figure 9. It is well-known that chemical stability of a molecule is largely affected by the frontier orbitals [31]. The highest occupied molecular orbital (HOMO) represents electron-donating capability, while the lowest unoccupied molecular orbital (LUMO) represents electron accepting capability. Thus, it is expected that the energy difference between the HOMO and LUMO (HOMO-LUMO energy gap) shows the chemical activity of the molecule. The calculated HOMO-LUMO energy gap of the title compound is 5.43 and 6.1 eV at the B3LYP and M06 levels, respectively. Hence, a relatively less kinetic stability is predicted for this molecule at the B3LYP level. Note that the relatively larger energy gap between the HOMO and LUMO of fentanyl at the M06 level compared to the B3LYP can be related to the large destabilization of the LUMO (Figure 9).

<Figure 9>

4.5. MEP analysis

The MEP analysis can be regarded as a powerful tool for identifying the possible interaction sites around a molecule [32-34]. Positive area of the MEP is indicative of a nucleophilic site, while negative region is associated with an electrophilic site. The MEP map of fentanyl is shown in Figure 10. One can see that the most negative region on the MEP map of fentanyl is associated with the lone-pairs of the oxygen atom with a value of -42 kcal/mol. This indicates that the oxygen atom of this molecule is the most reactive site to interact favorably with an acidic reagent in the protonation reaction. On the other hand, the MEP of fentanyl shows the presence of positive regions around the hydrogen atoms of phenyl groups, which clearly indicates the propensity of these sites for the formation of intermolecular interactions with potential electron-rich sites.

<Figure 10>

5. Conclusion

The title compound, fentanyl, was synthesized *via* one-pot reactions of 4-piperidonemonohydrochloride, phenylacetaldehyde, sodiumtriacetoxyborohydride, propionyl chloride. The structure of fentanyl was determined and characterized by elemental analysis, FT-IR, ^1H and ^{13}C NMR. The comparison between the calculated and experimental values indicated that the B3LYP/6-311++G(d,p) can predict the bond lengths, bond angles and dihedral angles of fentanyl better than the M06/6-311++G(d,p) method. In addition, it is found that the B3LYP calculated vibrational frequencies are in good agreement with the experimental FT-IR spectra. The MEP map of fentanyl predicts that the oxygen atom of fentanyl is the most reactive site to an electrophilic attack.

Acknowledgments

This work was supported by the *Sandoogh Hemayate az Pajuooheshgharane Keshvare Iran*.

References

- [1] A.F. Casy, R.T. Parfitt, *Opioid Analgesics*, Plenum Press, New York, 1986.
- [2] M. Williams, E.A. Kowaluk, S.P. Arneric, *J. Med. Chem.* 42 (1999) 1481.
- [3] W.F.M. Van Bever, C.J.E. Niemegeers, K.H.L. Schellekens, P.A.J. Janssen, *Arzneimittelforschung* 26 (1976) 1548.
- [4] O.M. Peeters, N.M. Blaton, C.J. De Ranter, A.M. Van Herk, K. Goubitz, *J. Cryst. Mol. Struct.* 9 (1979) 153.
- [5] S.H. Zee, W.K. Wang, *J. Chin. Chem. Soc.* 27 (1980) 147.
- [6] S.H. Zee, C.L. Lai, Y.M. Wu, G.S. Chen, *Nat. Sci. Council* 9 (1981) 387.
- [7] J. Guitton, M. Désage, S. Alamercery, L. Dutruch, S. Dautraix, J.P. Perdrix, J.L. Brazier, *J. Chromatogr. B* 59 (1997) 59.
- [8] Y.G. Suh, K.H. Cho, D.Y. Shin, *Arch. Pharmacol. Res.* 21 (1998) 70.
- [9] M. L. Jimeno, I. Alkorta, C. Cano, N. Jagerovic, P. Goya, J. Elguero, C. Foces-Foces, *Chem. Pharm. Bull.* 51 (2003) 929.
- [10] N. Ogawa, H. Nagase, T. Endo, T. Loftsson, H. Ueda, *X-Ray Struct. Anal. Online*, 25 (2009) 83.
- [11] A.F. Abdel-Magid, K.G. Carson, B.D. Harris, C.A. Maryanoff, R.D. Shah, *J. Org. Chem.* 61 (1996) 3849.
- [12] M.J. Frisch, G.W. Trucks, H.B. Schlegel, et al., *Gaussian 03, Revision 0.02*, Gaussian, Inc., Wallingford CT, 2004.
- [13] Y. Zhao, D.G. Truhlar, *Theor. Chem. Acc.* 120 (2008) 215–241.
- [14] K. Wolinski, J.F. Hinton, P. Pulay, *J. Am. Chem. Soc.* 112 (1990) 8251.
- [15] R.I.I. Dennington, T. Keith, J. Millam, *GaussView Version 4.1.2*, Semichem Inc., Shawnee Mission, KS, 2007.
- [16] N.M. O'Boyle, A.L. Tenderholt, K.M. Langner, *J. Comput. Chem.* 29 (2008) 839.
- [17] F. Bulat, A. Toro-Labbé, T. Brinck, J. Murray and P. Politzer, *J. Mol. Model.* 16 (2010) 1679.
- [18] C. B. Wade, D. K. Mohanty, P. J. Squattrito, N. J. Amato, K. Kirschbaum, *Acta Cryst. C* 69 (2013) 1383.
- [19] J. R. Deschamps, C. George, J. L. Flippen-Anderson, *Acta Cryst. C* 58 (2002) o362-o364.
- [20] R.R. Petrov, R.S. Vardanyan, G.S. Nichol, M.D. Carducci, S. Ma, J.Y. Lai, V.J. Hruby, *Acta Cryst. E* 62 (2006) o2815-o2816.
- [21] W.H.J. III, E.G. Buchanan, C.W. Müller, J.C. Dean, D. Kosenkov, L.V. Slipchenko, L. Guo, A.G. Reidenbach, S.H. Gellman, T.S. Zwier, *J. Phys. Chem. A* 115 (2011) 13783.

- [22] Y. Zhao, D.G. Truhlar, *Chem. Phys. Lett.* 502 (2011) 1.
- [23] P.R. Tentscher, J.S. Arey, *J. Chem. Theory Comput.* 8 (2012) 2165.
- [24] R. Valero, J.R.B. Gomes, D.G. Truhlar, F. Illas, *J. Chem. Phys.* 129 (2008) 124710.
- [25] M. Malik, D. Michalska, *Spectrochim. Acta Mol. Biomol. Spectrosc.* 125 (2014) 431.
- [26] V.K. Rastogi, M.A. Palafox, R.P. Tanwar, L. Mittal, *Spectrochimica. Acta A* 58 (2002) 1987.
- [27] R.M. Silverstein, G.C. Basseler and T.C. Morill, *Spectrometric Identification of Organic Compounds*, 4th ed. New York: John Wiley and Sons, 1981. QD272.S6 S55.
- [28] K. Helios, R. Wysokiński, A. Pietraszko, D. Michalska, *Vib. Spectrosc.* 55 (2011) 207.
- [29] C.A. Jiménez-Hoyos, B.G. Janesko and G.E. Scuseria, *Phys. Chem. Chem. Phys.* 10 (2008) 6621.
- [30] G.K. Hamer, I.R. Peat, W.F. Reynolds, *Can. J. Chem.* 51 (1973) 897.
- [31] E. Kavitha, N. Sundaraganesan, S. Sebastian, M. Kurt, *Spectrochim. Acta Mol. Biomol. Spectrosc.* 77 (2010) 612.
- [32] P. Politzer, D.G. Truhlar (Eds.), *Chemical Application of Atomic and Molecular Electrostatic Potentials*, Plenum, New York, 1981.
- [33] M.D. Esrafil, *Comput. Theor. Chem.* 1015 (2013) 1.
- [34] M.D. Esrafil, F. Mohammadian-Sabet, *Chem. Phys. Lett.* 628 (2015) 71.

Table 1. The experimental (Exp.) and calculated bond lengths (Å) of fentanyl at different levels of theory

| Bond length | Exp. | B3LYP/6- 311++G(d,p) | B3LYP/6- 311+G(d) | M06/6- 311++G(d,p) | M06/6- 311+G(d) |
|-------------|---------------------|-------------------------|----------------------|-----------------------|--------------------|
| C23-C24 | 1.39 ⁽¹⁾ | 1.39 | 1.39 | 1.38 | 1.38 |
| C24-C25 | 1.39 ⁽¹⁾ | 1.39 | 1.39 | 1.38 | 1.38 |
| C25-C20 | 1.40 ⁽¹⁾ | 1.40 | 1.40 | 1.39 | 1.39 |
| C22-C23 | 1.39 ⁽¹⁾ | 1.39 | 1.39 | 1.38 | 1.38 |
| C21-C22 | 1.39 ⁽¹⁾ | 1.39 | 1.39 | 1.38 | 1.38 |
| C20-C19 | 1.51 ⁽¹⁾ | 1.51 | 1.51 | 1.50 | 1.49 |
| C19-C18 | 1.54 ⁽¹⁾ | 1.54 | 1.53 | 1.52 | 1.52 |
| C18-N15 | 1.46 ⁽¹⁾ | 1.45 | 1.45 | 1.44 | 1.44 |
| N15-C14 | 1.46 ⁽²⁾ | 1.46 | 1.46 | 1.45 | 1.45 |
| C14-C13 | 1.52 ⁽²⁾ | 1.53 | 1.53 | 1.52 | 1.52 |
| C13-C12 | 1.54 ⁽²⁾ | 1.54 | 1.54 | 1.53 | 1.53 |
| C12-C17 | 1.54 ⁽²⁾ | 1.53 | 1.53 | 1.52 | 1.52 |
| C17-C16 | 1.54 ⁽²⁾ | 1.54 | 1.54 | 1.52 | 1.52 |
| C12-N7 | 1.48 ⁽²⁾ | 1.48 | 1.48 | 1.47 | 1.47 |
| N7-C1 | 1.44 ⁽²⁾ | 1.43 | 1.43 | 1.42 | 1.42 |
| N7-C8 | 1.36 ⁽²⁾ | 1.37 | 1.37 | 1.37 | 1.37 |
| C1-C6 | 1.39 ⁽²⁾ | 1.39 | 1.39 | 1.39 | 1.39 |
| C6-C5 | 1.39 ⁽²⁾ | 1.39 | 1.39 | 1.38 | 1.38 |
| C1-C2 | 1.38 ⁽²⁾ | 1.39 | 1.39 | 1.39 | 1.39 |
| C8-O9 | 1.22 ⁽²⁾ | 1.22 | 1.22 | 1.21 | 1.21 |
| C8-C10 | 1.51 ⁽²⁾ | 1.52 | 1.52 | 1.51 | 1.51 |
| C10-C11 | 1.49 ⁽²⁾ | 1.52 | 1.52 | 1.51 | 1.51 |

(1): *N*-(2-phenylethyl) nitroaniline [18].

(2): (1*R*)-2-[(3*R*,4*S*)-3-Methyl-4-(*N*-phenyl-*N*-propionylamino)piperidin-1-yl]-1-phenylethyl *p*-bromobenzoate and *N*-[(3*R*,4*S*)-1-[(2*S*)-2-(4-bromophenyl)-2-hydroxyethyl]-3-methyl-piperidin-4-yl]-*N*-phenylacrylamide [19].

Table 2. The experimental (Exp.) and calculated bond angles (°) of fentanyl at different levels of theory

| Bond angle | Exp. | B3LYP/6- 311++G(d,p) | B3LYP/6- 311+G(d) | M06/6- 311++G(d,p) | M06/6- 311+G(d) |
|-------------|----------------------|-------------------------|----------------------|-----------------------|--------------------|
| C20-C19-C18 | 111.0 ⁽¹⁾ | 111.9 | 111.9 | 110.8 | 110.8 |
| C19-C18-N15 | 112.6 ⁽¹⁾ | 113.2 | 113.3 | 113.4 | 113.4 |
| N15-C16-C17 | 110.7 ⁽²⁾ | 110.1 | 112.2 | 111.9 | 112.0 |
| C16-C17-C12 | 110.0 ⁽²⁾ | 110.6 | 110.1 | 109.7 | 109.7 |
| C17-C12-C13 | 110.4 ⁽²⁾ | 110.3 | 110.2 | 110.5 | 110.4 |
| C12-C13-C14 | 108.2 ⁽²⁾ | 110.6 | 110.7 | 110.1 | 110.2 |
| C12-N7-C1 | 111.6 ⁽²⁾ | 116.5 | 116.5 | 116.1 | 116.2 |
| C12-N7-C8 | 117.1 ⁽²⁾ | 120.9 | 120.9 | 121.0 | 121.0 |
| N7-C8-O9 | 122.1 ⁽²⁾ | 121.5 | 121.6 | 121.8 | 121.9 |
| C8-C10-C11 | 112.2 ⁽²⁾ | 112.4 | 112.4 | 112.3 | 112.4 |
| O9-C8-C10 | 121.7 ⁽²⁾ | 121.3 | 121.3 | 121.8 | 121.8 |
| C1-N7-C8 | 122.0 ⁽²⁾ | 122.4 | 122.4 | 122.7 | 122.6 |

(1): *N*-(2-phenylethyl) nitroaniline [18].

(2): (1*R*)-2-[(3*R*,4*S*)-3-Methyl-4-(*N*-phenyl-*N*-propionylamino)piperidin-1-yl]-1-phenylethyl *p*-bromobenzoate and *N*-{(3*R*,4*S*)-1-[(2*S*)-2-(4-bromophenyl)-2-hydroxyethyl]-3-methyl-piperidin-4-yl}-*N*-phenylacrylamide [19].

Table 3. The experimental (Exp.) and calculated dihedral angles ($^{\circ}$) of fentanyl at different levels of theory

| Dihedral angle | Exp. | B3LYP/ 6-311++G(d,p) | B3LYP/6-311+G(d) | M06/6-311++G(d,p) | M06/6-311+G(d) |
|-----------------|----------------------|----------------------|------------------|-------------------|----------------|
| C16-C17-C12-C13 | -54.4 ⁽¹⁾ | -62.1 | -62.1 | -62.8 | -62.7 |
| C18-N15-C14-C13 | 167.9 ⁽¹⁾ | 162.0 | 162.5 | 163.2 | 163.6 |
| C12-N7-C1-C2 | -96.3 ⁽¹⁾ | -80.7 | -80.8 | -80.6 | -80.6 |
| C16-C17-C12-C13 | -54.5 ⁽²⁾ | -62.1 | -62.1 | -62.8 | -62.7 |
| C17-C12-C13-C14 | -54.9 ⁽²⁾ | 28.4 | 28.2 | 28.9 | 28.4 |
| C12-C13-C14-N15 | 58.9 ⁽²⁾ | 34.3 | 34.5 | 34.5 | 34.9 |
| C18-N15-C14-C13 | 167.9 ⁽²⁾ | 162.0 | 162.4 | 163.2 | 163.5 |
| C17-C12-N7-C8 | 157.9 ⁽²⁾ | 62.9 | 63.0 | 62.5 | 62.7 |
| C17-C12-N7-C1 | -14.2 ⁽²⁾ | -115.9 | -115.9 | -114.5 | -114.5 |
| C12-N7-C8-O9 | 4.4 ⁽²⁾ | -0.8 | -1.0 | -0.1 | -0.3 |
| C12-N7- C1-C2 | -96.3 ⁽²⁾ | -80.7 | -80.7 | -80.6 | -80.5 |

(1): 4-{*N*-[2-(1,3-Dioxo-1,3-dihydroisoindol-2-yl)-3-phenylpropionyl]anilino}-1-phenethylpiperidinium chloride methanol.disolvate [20].

(2): (1*R*)-2-[(3*R*,4*S*)-3-Methyl-4-(*N*-phenyl-*N*-propionylamino)piperidin-1-yl]-1-phenylethyl *p*-bromobenzoate and *N*-[(3*R*,4*S*)-1-[(2*S*)-2-(4-bromophenyl)-2-hydroxyethyl]-3-methyl-piperidin-4-yl]-*N*-phenylacrylamide [19].

Table 4. Calculated Mullikan atomic charges (e) of fentanyl

| atom | B3LYP/6- 311++G(d,p) | B3LYP/6- 311+G(d) | M06/6- 311++G(d,p) | M06/6- 311+G(d) |
|------|-------------------------|----------------------|-----------------------|--------------------|
| C20 | 1.047 | 1.495 | 0.740 | 1.153 |
| C19 | -0.534 | -1.074 | -0.671 | -1.045 |
| C18 | -0.682 | -0.800 | -0.220 | -0.664 |
| N15 | 0.277 | 0.525 | -0.006 | 0.275 |
| C16 | -0.298 | -0.722 | -0.051 | -0.524 |
| C17 | -0.337 | -0.576 | -0.047 | -0.298 |
| C12 | -0.853 | -1.023 | -1.570 | 1.675 |
| C13 | 0.106 | -0.015 | 0.412 | 0.091 |
| C14 | -0.468 | -0.783 | -0.275 | -0.711 |
| N7 | 0.816 | 0.861 | 0.439 | 0.452 |
| C1 | -0.432 | -0.406 | -0.216 | 0.204 |
| C8 | -0.062 | 0.074 | -0.057 | 0.090 |
| O9 | -0.211 | -0.276 | -0.217 | -0.274 |
| C10 | -0.225 | -0.331 | -0.159 | -0.383 |
| C11 | -0.638 | -1.057 | -0.518 | -1.050 |

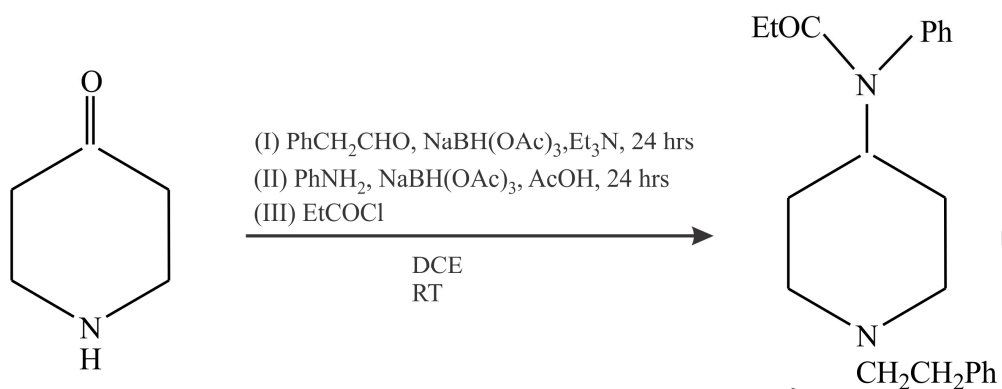
Table 5. Calculated (δ_{cal}) and experimental (δ_{exp}) ^1H chemical shifts of fentanyl

| Atom | Calculated | | | | δ_{exp} |
|------|---------------------|---|-------------------|---|-----------------------|
| | B3LYP/6-311++G(d,p) | $\delta_{\text{exp}} - \delta_{\text{B3LYP}}$ | M06/6-311++G(d,p) | $\delta_{\text{exp}} - \delta_{\text{M06}}$ | |
| H33 | 0.58 | 0.45 | 1.33 | -0.30 | 1.03 -1.06 |
| H34 | 0.88 | 0.16 | 1.76 | -0.72 | - |
| H35 | 1.24 | -0.18 | 2.00 | -0.94 | - |
| H32 | 1.61 | 0.32 | 2.42 | -0.49 | 1.93-1.98 |
| H43 | 1.62 | 0.36 | 2.22 | -0.24 | |
| H31 | 1.89 | -0.42 | 2.47 | -1.00 | 1.47 – 1.49 |
| H45 | 2.27 | -0.44 | 2.87 | -1.04 | |
| H38 | 2.28 | 0.75 | 2.91 | 0.12 | 1.85 – 1.83 |
| H41 | 2.31 | -0.13 | 2.77 | -0.59 | |
| H40 | 2.43 | 0.13 | 2.95 | -0.39 | 2.23 – 2.18 |
| H46 | 2.50 | -0.65 | 2.99 | -1.14 | |
| H47 | 2.56 | -0.33 | 3.00 | -0.77 | 2.59 – 2.56 |
| H48 | 2.76 | -0.01 | 3.48 | -0.73 | |
| H37 | 2.88 | -0.29 | 3.29 | -0.70 | 2.78 – 2.75 |
| H39 | 2.93 | -0.15 | 3.49 | -0.71 | |
| H42 | 3.18 | -0.13 | 3.71 | -0.66 | 3.05 – 3.03 |
| H36 | 3.42 | 1.30 | 4.02 | 0.70 | 4.71 |
| H44 | 3.50 | -2.01 | 4.31 | -2.82 | 3.05 – 3.03 |
| H49 | 7.30 | -0.20 | 8.05 | -0.95 | 7.10- 7.42 |
| H50 | 7.33 | -0.22 | 8.31 | -1.20 | - |
| H51 | 7.37 | -0.23 | 7.95 | -0.81 | - |
| H53 | 7.42 | -0.24 | 8.05 | -0.87 | - |
| H30 | 7.42 | -0.22 | 8.04 | -0.84 | - |
| H52 | 7.48 | -0.23 | 8.08 | -0.83 | - |
| H26 | 7.48 | -0.23 | 8.16 | -0.91 | - |
| H29 | 7.50 | 0.45 | 8.34 | -1.06 | - |
| H28 | 7.55 | 0.16 | 7.95 | -0.65 | - |
| H27 | 7.71 | -0.18 | 8.6 | -1.18 | - |

Table 6. Calculated (δ_{cal}) and experimental (δ_{exp}) ^{13}C NMR chemical shifts of fentanyl

| Atom | Calculated | | | | δ_{exp} |
|------|---------------------|---|-------------------|---|-----------------------|
| | B3LYP/6-311++G(d,p) | $\delta_{\text{exp}} - \delta_{\text{B3LYP}}$ | M06/6-311++G(d,p) | $\delta_{\text{exp}} - \delta_{\text{M06}}$ | |
| C11 | 10.93 | -1.35 | 10.62 | -1.04 | 9.58 |
| C17 | 28.04 | -5.47 | 27.95 | -5.38 | 22.57 |
| C13 | 31.11 | -2.62 | 28.08 | 0.41 | 28.49 |
| C10 | 34.25 | -3.69 | 33.07 | -2.51 | 30.56 |
| C19 | 42.33 | -8.51 | 42.05 | -8.23 | 33.82 |
| C16 | 56.55 | -4.41 | 55.34 | -3.2 | 52.14 |
| C14 | 57.03 | -3.95 | 55.54 | -2.46 | 53.08 |
| C12 | 65.86 | -5.4 | 66.13 | -5.67 | 60.46 |
| C18 | 69.20 | - | 70.98 | - | - |
| C23 | 131.89 | -5.91 | 134 | -8.02 | 125.98 |
| C4 | 133.91 | -5.7 | 135.18 | -6.97 | 128.21 |
| C22 | 134.39 | -6.05 | 136.31 | -7.97 | 128.34 |
| C24 | 135.02 | -6.43 | 136.15 | -7.56 | 128.59 |
| C21 | 135.93 | -6.69 | 137.00 | -7.76 | 129.24 |
| C2 | 136.03 | -5.62 | 138.02 | -7.61 | 130.41 |
| C25 | 135.09 | - | 140.00 | - | - |
| C5 | 135.76 | - | 137.23 | - | - |
| C6 | 136.19 | - | 138.23 | - | - |
| C3 | 137.24 | 1.61 | 138.50 | 0.35 | 138.85 |
| C20 | 149.95 | -9.71 | 149.29 | -9.05 | 140.24 |
| C1 | 155.97 | - | 155.82 | - | - |
| C8 | 178.92 | -5.42 | 183.00 | -9.5 | 173.5 |

†



Scheme 1. One pot synthesis of fentanyl via reductive alkylation and amination reaction in the presence of sodium triacetoxyborohydride (STAB)

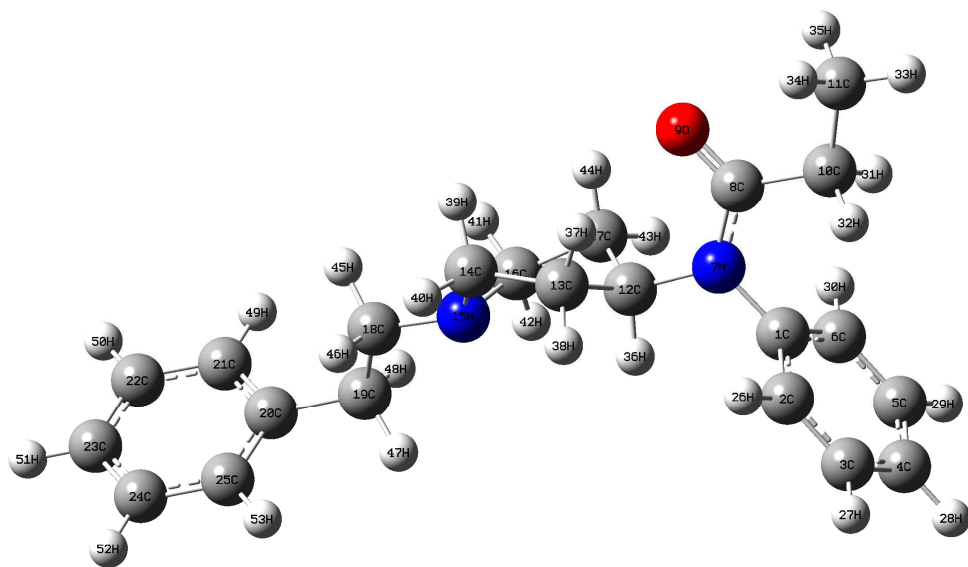


Figure 1. The optimized structure of fentanyl

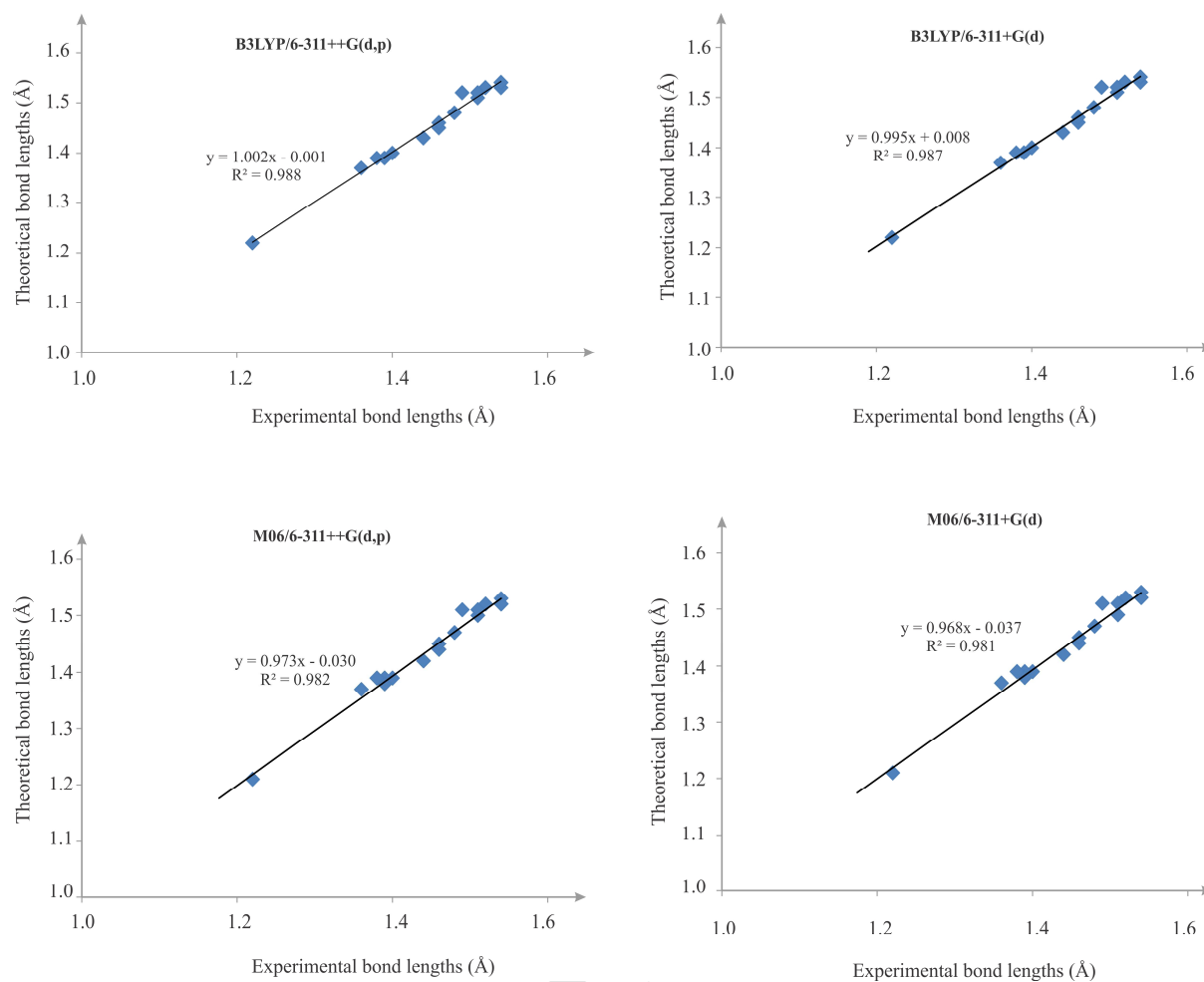


Figure 2. Linear correlations between the experimental and calculated bond lengths of fentanyl

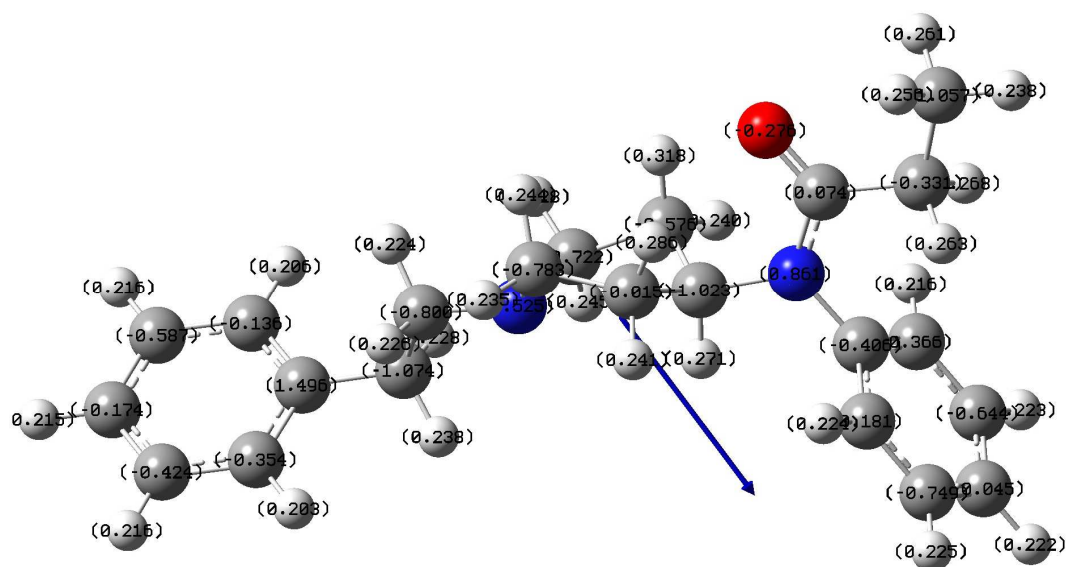


Figure 3. Atomic Mulliken charges and orientation of the dipole moment of fentanyl calculated at the B3LYP/6-31++G(d,p) level

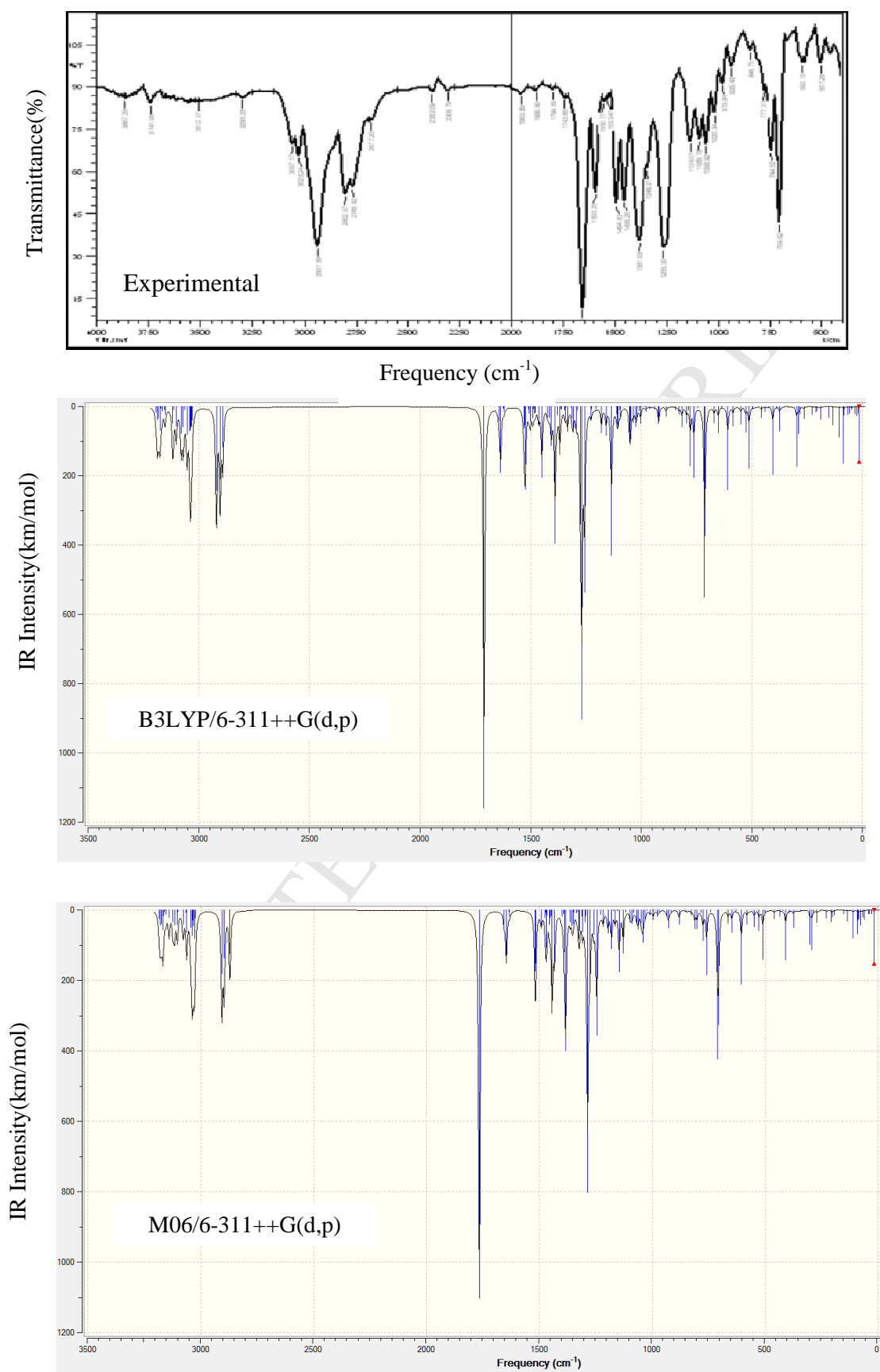


Figure 4. The experimental and calculated IR spectra of fentanyl

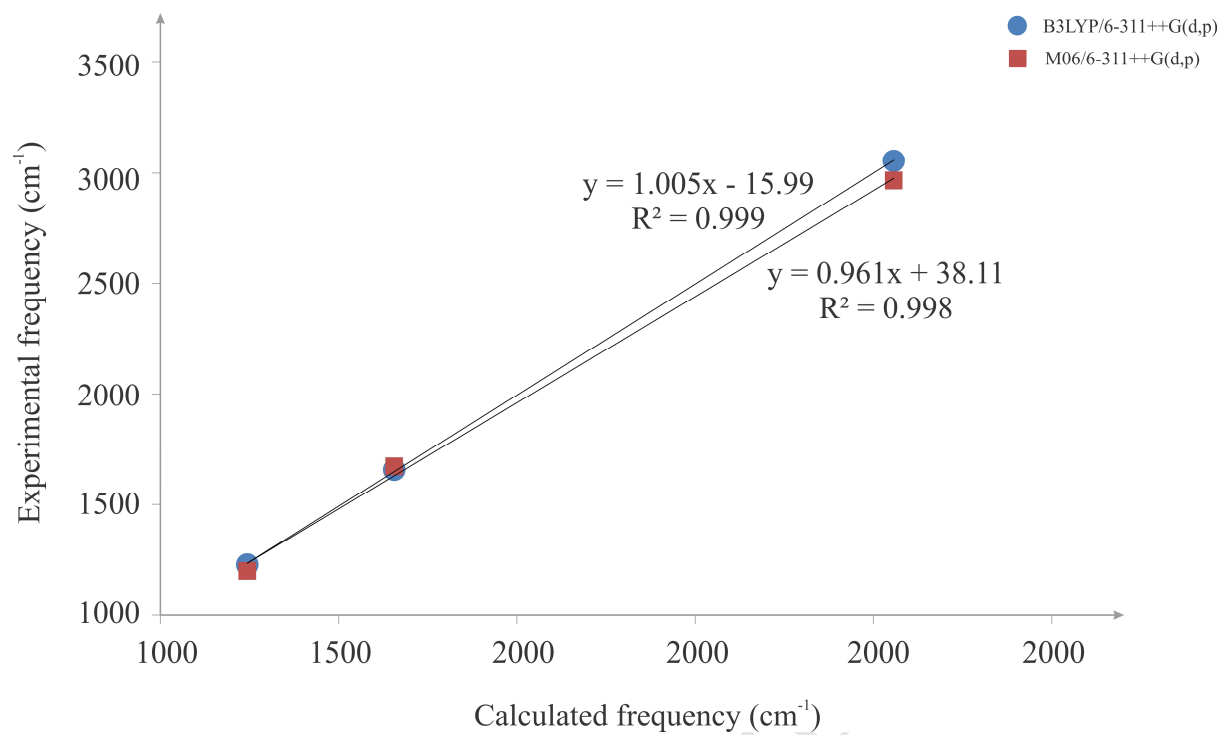


Figure 5. Relationship between the experimental and calculated frequencies of fentanyl

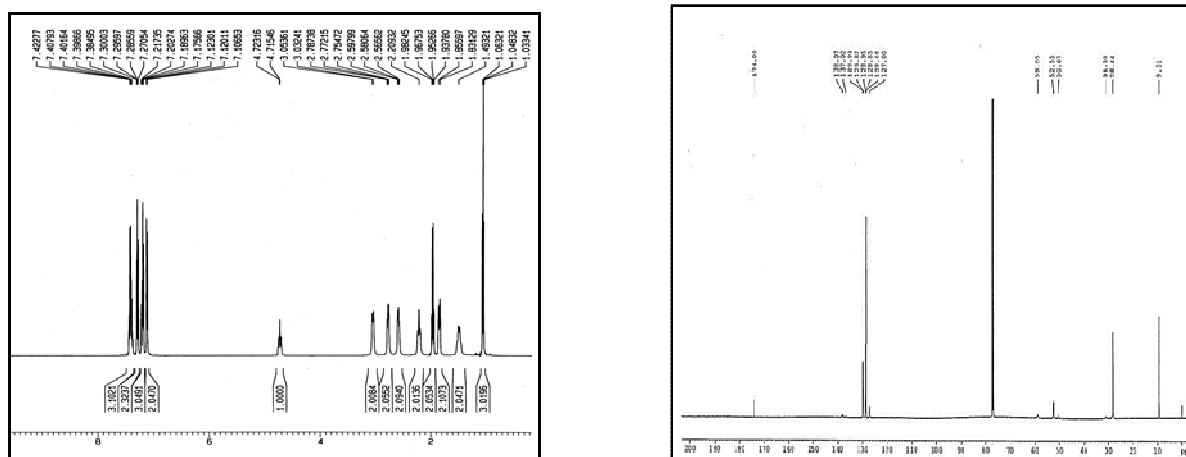


Figure 6. Experimental ^1H (left) and ^{13}C (right) chemical shifts of fentanyl

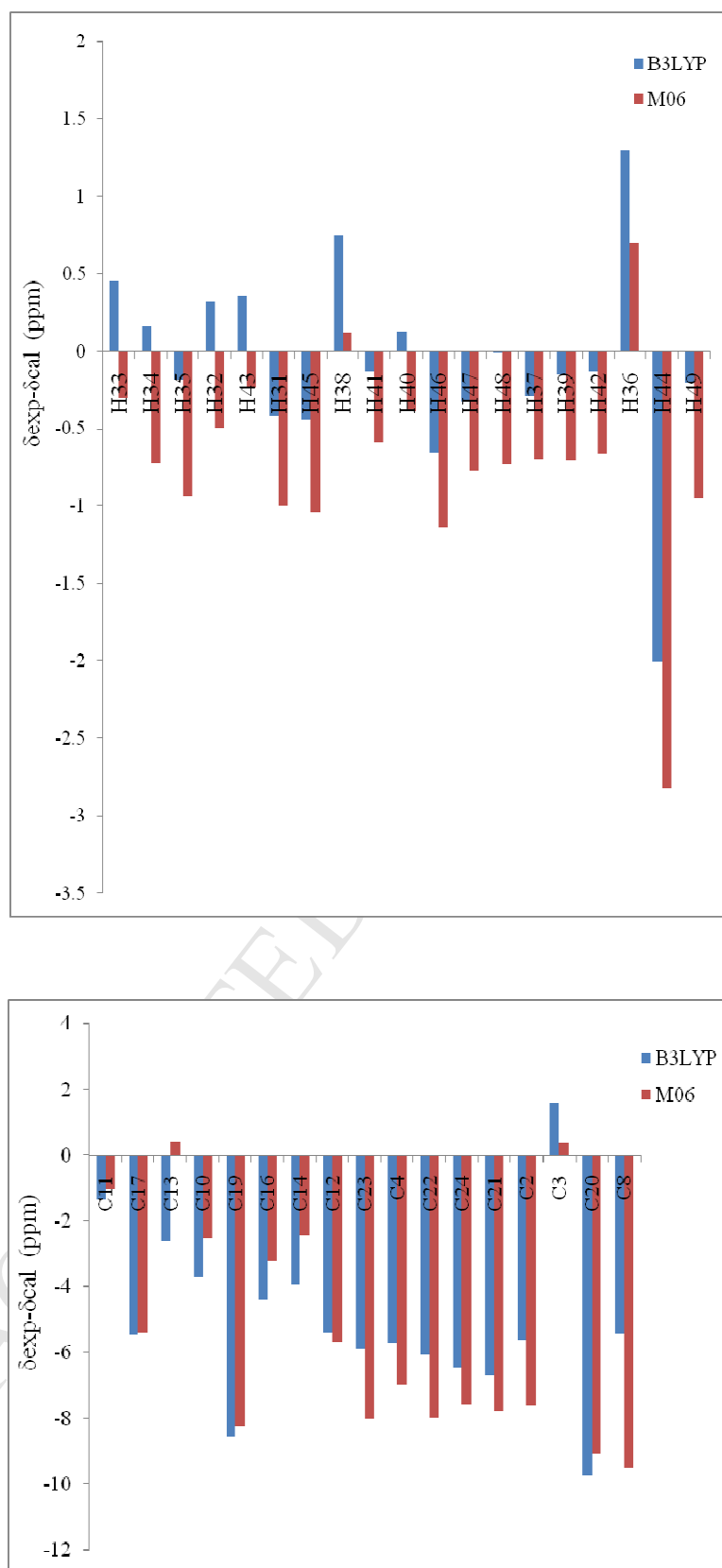


Figure 7. The deviation of calculated ^1H (above) and ^{13}C (below) chemical shifts from the corresponding experimental values

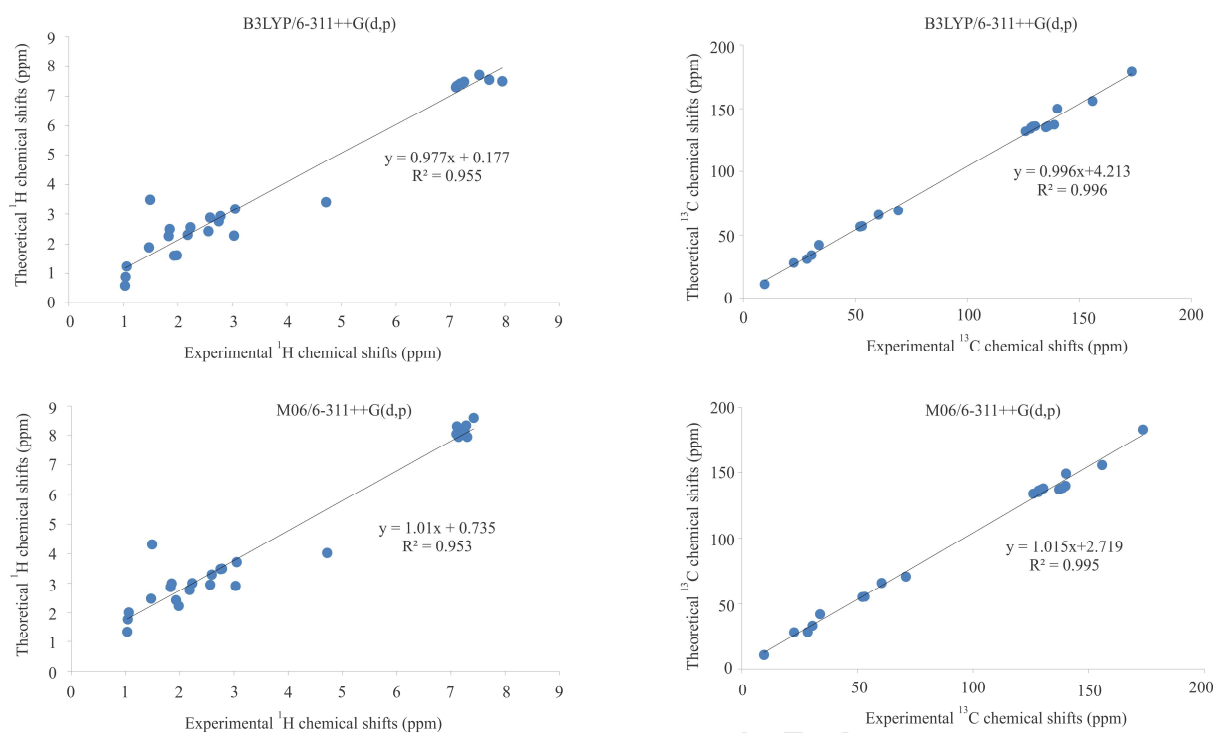


Figure 8. Correlation between the experimental and calculated ^1H and ^{13}C chemical shifts of fentanyl

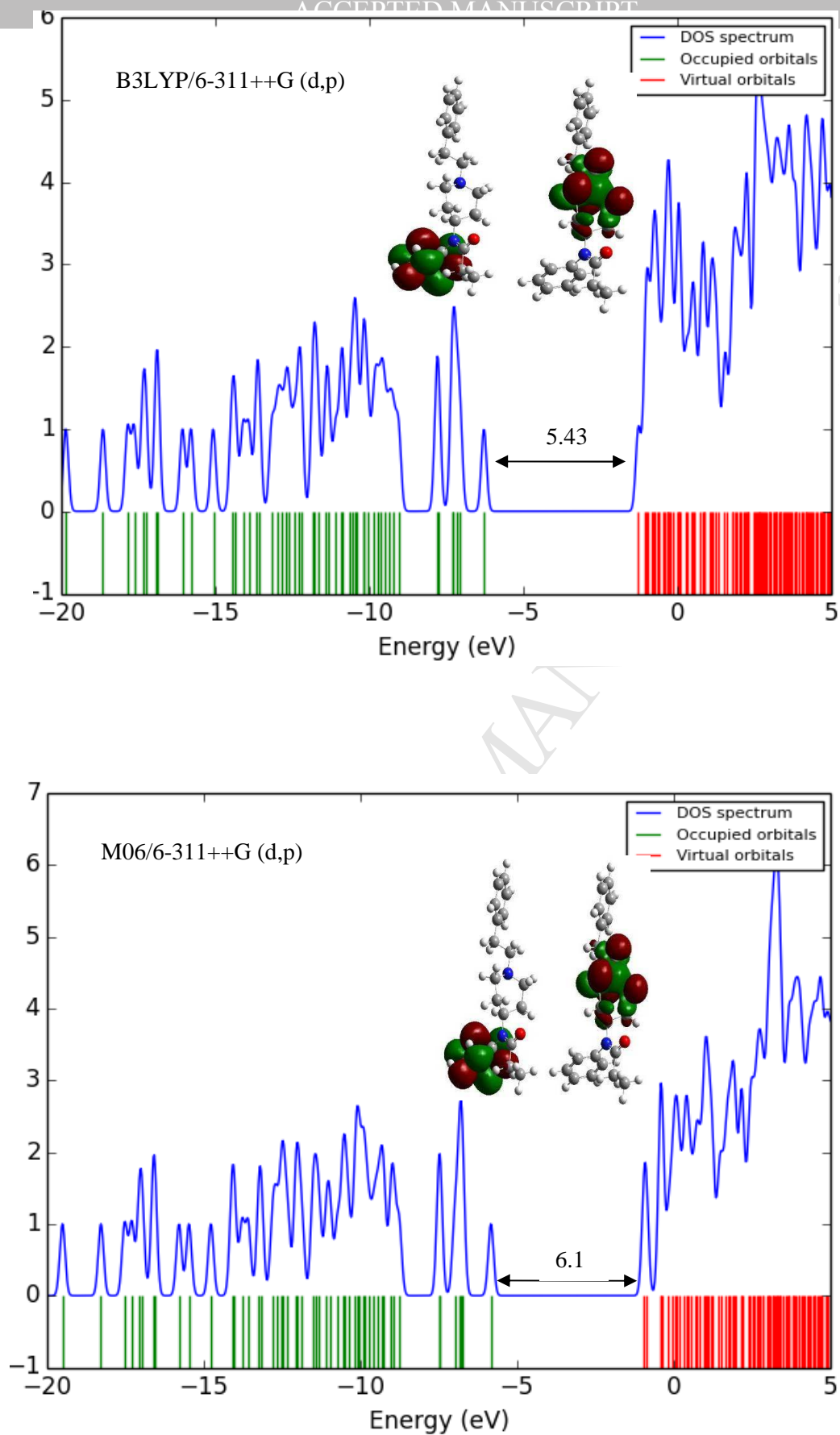


Figure 9. DOS diagram, HOMO (left) and LUMO (right) of fentanyl

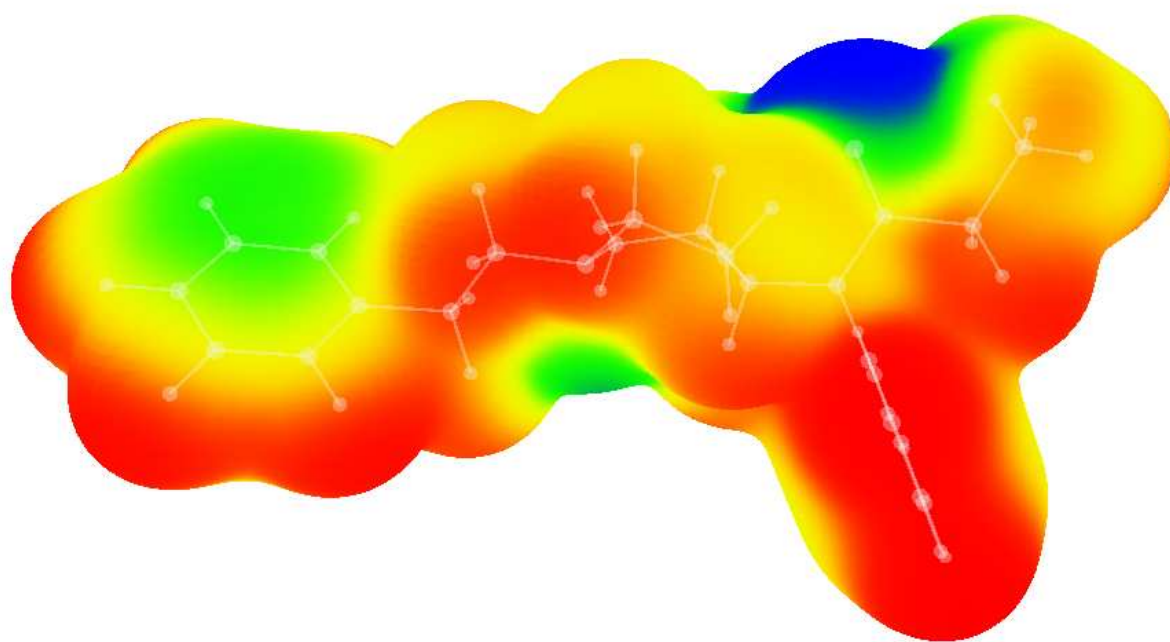


Figure 10. The molecular electrostatic potential (MEP) of fentanyl. The color range, in kcal/mol, is: red > 4.5 , $4.5 > \text{yellow} > -11.0$, $-11.0 > \text{green} > -26.6$ and blue < -26.6 .

Research highlights:

- 1) An efficient method for preparation of fentanyl via an one-pot reaction is introduced.
- 2) Almost a good linear correlation is obtained between the B3LYP/6-311++G(d,p) results and experimental data.
- 3) The oxygen atom of fentanyl is the most reactive site to an electrophilic attack.